Molecular Therapy
Nucleic Acids
Original Article

A novel DNA aptamer targeting lung cancer stem cells exerts a therapeutic effect by binding and neutralizing Annexin A2

Yi-Ying Wu,[1,2,7] I-Shan Hsieh,[3,7] Chia-Hao Tung,[2] Chen-Hsun Weng,[4] Jia-En Wu,[2] Jau-Song Yu,[5,6] Tse-Ming Hong,[1,2] and Yuh-Ling Chen[3]

[1]Clinical Medicine Research Center, National Cheng Kung University Hospital, College of Medicine, National Cheng Kung University, Tainan 704302, Taiwan; [2]Institute of Clinical Medicine, National Cheng Kung University, No. 1 University Road, Tainan 70101, Taiwan; [3]Institute of Oral Medicine, National Cheng Kung University, No. 1 University Road, Tainan 70101, Taiwan; [4]Medical Device Innovation Center, National Cheng Kung University, Tainan 704302, Taiwan; [5]Graduate Institute of Biomedical Sciences, College of Medicine, Chang Gung University, Tao-Yuan 333323, Taiwan; [6]Molecular Medicine Research Center, Chang Gung University, Tao-Yuan 333323, Taiwan

Cancer remains one of the leading causes of death worldwide. Cancer stem cells (CSCs) are the underlying reason for tumor recurrence, progression, and therapeutic resistance. Aptamers are synthetic single-stranded oligonucleotides that can specifically bind to various molecular targets. Here, we aim to develop an effective aptamer-based biomarker and therapeutic tool that targets CSCs for cancer therapy. We perform whole-cell-based systematic evolution of ligands by exponential enrichment (cell-SELEX) to screen DNA aptamers that specifically bound to lung CSCs, modeled by E-cadherin-silenced A549 cells. We develop a CSC-specific aptamer (AP-9R) specifically recognizing lung CSCs with high affinity and identify Annexin A2, a Ca^{2+}-dependent membrane-binding protein, as its target. Annexin A2 expression was upregulated in lung CSCs and involved in cancer stemness. The expression of Annexin A2 was associated with signatures of stemness and metastasis, as well as poor clinical outcomes, in lung cancer *in silico*. Moreover, AP-9R decreased Annexin A2 expression and suppressed CSC properties in CSCs *in vitro* and *in vivo*. The present findings suggest that Annexin A2 is a CSC marker and regulator, and the CSC-specific aptamer AP-9R has potential theranostic applications for lung cancer.

INTRODUCTION

Cancer is a common disease in humans and is one of the leading causes of death worldwide. Recently, it has been found that a small subpopulation of cancer cells, called cancer stem cells (CSCs) or tumor-initiating cells (TICs), has the exclusive ability to self-renew and generate differentiated cancer cell progeny that comprise the tumor and cause tumor heterogeneity.[1] CSCs are characterized by Hoechst exclusion, aldehyde dehydrogenase (ALDH) activity, or the expression of several specific markers that differ among cancer types. Increasing amounts of evidence have shown that CSCs play a role in creating a particular niche for metastasis and have the advantage of apparent therapeutic resistance.[2–4] Current anticancer therapies mostly fail to eradicate CSC clones and instead promote the expansion of the CSC pool and/or the selection of resistant CSC clones, thus leading to a fatal disease outcome. Therefore, targeting CSCs may facilitate the complete eradication of cancer and the improvement of clinical outcomes. However, CSCs are rare, and current methods to identify and characterize CSCs are limited because CSCs quickly differentiate into other cell types. Therefore, the identification of surface markers and related genes for the identification of these CSCs urgently needs to be pursued. The enrichment of CSCs can be helpful in the screening of therapeutic agents that exclusively target CSCs.

Aptamers are single-stranded DNA (ssDNA) or RNA (ssRNA) oligonucleotide ligands that specifically bind to various molecular targets, and the use of aptamers as biomaterials, diagnostic and therapeutic tools, or for the development of new drug delivery systems has been investigated in numerous studies.[5,6] Aptamers can discriminate between closely related targets with high specificity and affinity (dissociation constant [K_D] = pM ∼ nM).[7] In addition to the specific recognition of their targets, aptamers also possess several advantages over antibodies, such as high stability, ease of synthesis, low immunogenicity, and diverse target.[8] Moreover, aptamers are amenable to chemical modification and bioconjugation to various moieties, such as nanoparticles, imaging agents, small interfering RNAs (siRNAs), and therapeutic drugs.[9] Based on all of these advantages, aptamers are considered to be an alternative to antibodies and to have great potential as molecular probes for cancer diagnosis and treatment. To date, 11 RNA or DNA aptamers have entered the clinical

Received 11 July 2021; accepted 17 January 2022;
https://doi.org/10.1016/j.omtn.2022.01.012.

[7]These authors contributed equally

Correspondence: Tse-Ming Hong, PhD, Institute of Clinical Medicine, National Cheng Kung University, No. 1 University Road, Tainan 70101, Taiwan.
E-mail: tmhong@mail.ncku.edu.tw
Correspondence: Yuh-Ling Chen, PhD, Institute of Oral Medicine, National Cheng Kung University, No. 1 University Road, Tainan 70101, Taiwan.
E-mail: yuhling@mail.ncku.edu.tw

development pipeline for treating several diseases.[10] Recent studies have also reported that a panel of target-specific aptamers selected by a cell-based systematic evolution of ligands by the exponential enrichment (cell-SELEX) selection method exhibit high affinity and selectivity for cancer cells.[10–13] However, there is still a lack of research on CSC-specific aptamers and their applications.

Increasing numbers of reports suggest that the malignant cancer cells undergoing epithelial-mesenchymal transition (EMT) simultaneously possess stemness properties. EMT programs promote CSC stemness in many epithelial tumors.[14,15] Previous studies have reported that the successful preparation of CSCs depends on developing a stable *in vitro* stem cell culture by inhibiting the expression of E-cadherin in cancer cells.[2] Thus, we used an E-cadherin-silenced lung cancer cell model, A549^{shEcad}, in which E-cadherin expression was knocked down by a lentiviral short hairpin RNA (shRNA) strategy and exhibited stem cell properties, and the cell-SELEX selection method to screen high-affinity aptamers specific for CSCs. We found a CSC-specific aptamer, AP-9R, and identified its target, Annexin A2, as a CSC surface marker and a regulator of cancer migration and stemness. AP-9R can be utilized for CSC capture and has potential as a cancer therapeutic agent.

RESULTS

Isolation and characterization of CSC-specific DNA aptamers

By gene set enrichment analysis (GSEA) of The Cancer Genome Atlas lung adenocarcinoma cohort (TCGA-LUAD, $n = 517$),[16] E-cadherin expression (CDH1) was found to be inversely correlated with stem cell signatures (Figure S1A). Indeed, previous studies have reported that the successful preparation of CSCs depends on developing a stable *in vitro* stem cell culture by first inhibiting E-cadherin expression.[2] Here, we used E-cadherin-specific lentiviral shRNAs to generate stable E-cadherin-knockdown lung cancer cells. Two lentiviral shRNAs, designated shEcad#1 and shEcad#2, and a lentiviral shRNA specific for the firefly luciferase gene, shLuc (luciferase shRNA; as a control), were transduced into A549 cells. After infection, the shEcad-infected cells (A549^{shEcad}) exhibited a significant reduction in E-cadherin expression and increased vimentin expression compared with the shLuc-infected cells (A549^{shLuc}). Notably, the A549^{shEcad} cells exhibited a substantial increase in the expression of stem cell markers, such as Nestin, Nanog, and Oct-4 (Figure S1B). We further used a sphere formation assay to confirm that A549^{shEcad} cells have increased stem-cell-like properties (Figure S1C). Although the sphere cells were recovered to the adhesive culture condition, A549^{shEcad} cells still presented the increased expression levels of stem cell markers, compared with A549^{shLuc} cells, so the cancer stemness properties of A549^{shEcad} cells could be maintained (Figure S1D). We also assessed the functional presence of stem-like CSCs by depleting E-cadherin *in vivo*. A549^{shEcad} cells were subcutaneously injected into nonobese diabetic/severe combined immunodeficiency (NOD/SCID) mice, and A549^{shLuc} cells were injected as controls. Consistent with the *in vitro* observations, the inhibition of E-cadherin increased the tumor initiation rate (Table S1) and tumor growth rate (Figure S1E). A549 cells with silenced E-cadherin exhibited CSC properties.

Then, we used cell-SELEX to screen high-affinity DNA aptamers for targeting CSCs.[17,18] A549^{shEcad} cells were used as the target cells, and A549^{shLuc} cells were used for negative selection (Figure 1A). We started the first cycle selection with 100 pmol random 40-mer ssDNA libraries flanked with two 16-mer primers. We performed 15 cycles to produce enriched high-affinity ssDNA pools in sufficient quantities to finish the selection. After 15 rounds of selection, the enriched DNA pool was cloned and sequenced. Individual clones were tested for their ability to bind to A549^{shEcad} and A549^{shLuc} cells. One of the resulting aptamers, AP-9R, was demonstrated to have a higher binding affinity for CSC-like A549^{shEad} cells than A549^{shLuc} cells (Figure 1B). The potential secondary structures of AP-9R were predicted by using MFOLD software version 3.5 (available at: http://mfold.rna.albany.edu/). To quantitatively evaluate the binding affinity of AP-9R to A549^{shEcad} cells, we incubated A549^{shEcad} cells with increasing concentrations of Fluorescein amidite (FAM)-labeled AP-9R and analyzed them by flow cytometry. Using nonlinear regression analysis, the calculated K_D of AP-9R for A549^{shEcad} cells was 54.29 ± 9.55 nM (Figure 1C).

We then evaluated the possibility of using AP-9R as a biomarker detector to detect lung CSCs. First, the epithelial surface marker, EpCAM (epithelial cell adhesion molecule), was detected in the normal lung cell line BEAS-2B and increased in A549 cells by flow cytometry analysis, while A549^{shLuc} and A549^{shEcad} cells exhibited the similar EpCAM levels (Figure S1F). Next, the specificity of AP-9R was further tested by analyzing the binding of FAM-labeled aptamers to target cells, control cells, and other lung normal cell lines. As shown in Figure 1D, AP-9R could bind to the target A549^{shEad} cells, but not the control A549^{shLuc} cells or the normal lung cell line BEAS-2B. The scrambled aptamer (control) and the initial library could not distinguish the three cell types. In addition, the binding of AP-9R to A549^{shEad} cells was also verified by confocal microscopy (Figure 1E). We found that AP-9R was localized not only at the cell membrane but also in the cytoplasm and nuclei. The uptake of AP-9R by A549^{shEad} cells was blocked by the endocytic inhibitor chlorpromazine (Figure S2). This result indicates that AP-9R may bind to its cell surface target and subsequently be internalized into cells. Taken together, we identified the DNA aptamer AP-9R, which specifically binds to CSC-like lung cancer cells with a nanomolar K_D.

Identification of the AP-9R-targeted protein

To identify the AP-9R target on A549^{shEad} cells, we used biotin-labeled AP-9R and streptavidin-conjugated beads to pull down the surface proteins that bound to AP-9R in the membrane fraction of A549^{shEcad} cell lysates, and the AP-9R-specific binding proteins were identified by mass spectrometry (Figure 2A). We found that AP-9R specifically interacted with a protein with a molecular mass of approximately 38 kDa (Figure S3). Thus, the 38-kDa polypeptide band was excised and analyzed by mass spectrometry. Among the significant protein hits (Table S2), the possible AP-9R-targeted protein was Annexin A2 (*ANXA2*), which was identified among the AP-9R binding proteins in membrane fractions from A549^{shEcad} cells with 27 unique peptides. Indeed, Annexin A2 was observed in the biotin-labeled AP-9R

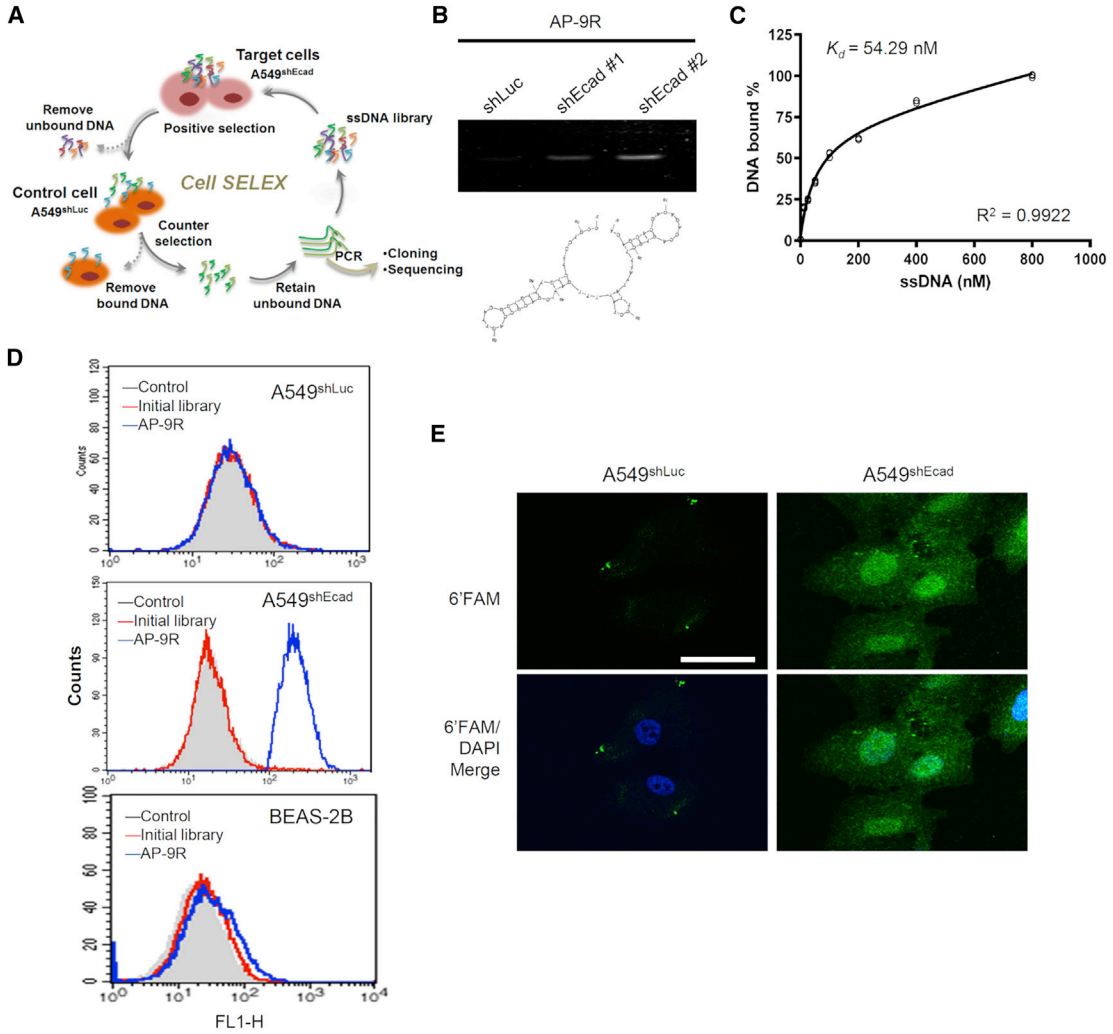

Figure 1. Isolation and characterization of cancer stem-cell-specific DNA aptamers

(A) Schema of the cell-SELEX procedure. (B) Binding specificity and the predicted secondary structure of AP-9R, a cancer stem-cell-specific DNA aptamer. The binding ability of AP-9R against A549 cells infected with lentiviruses carrying E-cadherin shRNAs (shEcad#1 and shEcad#2) or luciferase shRNA (shLuc) was determined by PCR amplification. (C) Binding curves of varying concentrations of FAM-labeled AP-9R aptamer (0–800 nM) in shEcad-transduced A549 cells. Experiment was performed in triplicate. The actual fluorescence intensity was fitted to SigmaPlot software to determine the dissociation constant (K_D). (D) A representative flow cytometric binding analysis of FAM-labeled AP-9R to shLuc- and shEcad-infected A549 (A549^{shLuc} and A549^{shEcad}) and bronchial epithelial cells BEAS-2B. (E) The binding of FAM-labeled AP-9R to A549^{shLuc} and A549^{shEcad} cells was determined by confocal imaging of the immunofluorescence. The nuclei were visualized by DAPI staining (blue). Scale bars: 20 μm.

pull-down complex, but not in the biotin-labeled initial library pull-down complex from A549^{shEcad} cell lysate (Figure 2B). Moreover, elevated expression of Annexin A2 in CSC-like lung cancer cells was also observed, including in A549^{shEcad} cells, side populations (SPs) of A549 and CLS1 cells, and ALDH-positive CLS1 cells (Figures 2C and S4A).

Next, we determined whether AP-9R binds to A549^{shEcad} cells through Annexin A2, and lentiviral shRNA for Annexin A2 (shANXA2) was used. After infection, shANXA2-infected A549^{shEcad} cells (A549$^{shEcad/AnxA2}$) had an obvious reduction in Annexin A2 expression by western blot analysis and flow cytometry analysis (Figures 2D and S4B). When FAM-labeled AP-9R was incubated with A549$^{shEcad/AnxA2}$ cells, the fluorescence became weak and even undetectable as observed by flow cytometry analysis (Figure 2E). Consistently, by immunofluorescence experiments, FAM-labeled AP-9R was strongly detected in A549^{shEcad} cells but weakly detected in A549$^{shEcad/AnxA2}$ cells (Figure 2F). The levels of cells stained with FAM-labeled AP-9R correlated with the expression levels of Annexin A2 in cells. Therefore, FAM-labeled AP-9R could be stained on Annexin A2-expressed cells. These data suggest that Annexin A2 is a protein target of AP-9R, and that AP-9R targets cancer stem-like cells by directly binding to Annexin A2.

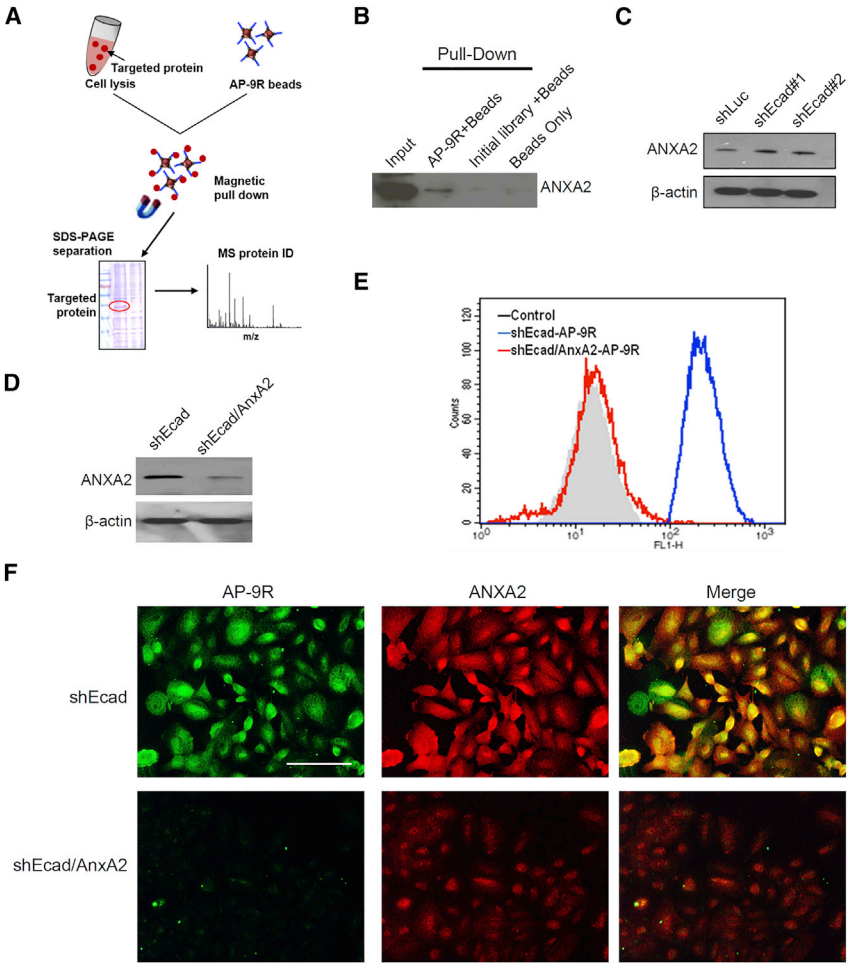

Figure 2. Annexin A2 mediates the binding of AP-9R to E-cadherin-knockdown A549 cells

(A) Schematic of the strategy for identifying AP-9R binding proteins. (B) Pull-down assay of AP-9R. Whole-protein lysates of A549^{shEcad} cells were incubated with biotin-labeled AP-9R and then pulled down by streptavidin-coated magnetic beads. The precipitated proteins were analyzed by western blotting using an anti-Annexin A2 (ANXA2) antibody. (C and D) Western blotting of ANXA2 in A549 cells transfected with shLuc or shEcad (C) and A549^{shEcad} cells infected with an ANXA2-specific shRNA (D). β-Actin was used as the loading control. (E) A representative flow cytometric analysis of FAM-labeled AP-9R binding to ANXA2-knockdown A549^{shEcad} cells. (F) Cellular colocalization of FAM-labeled AP-9R (green) and ANXA2 (red) was determined by fluorescence microscopy in E-cadherin-knockdown (shEcad) A549 cells and in A549 cells with double knockdown of E-cadherin and ANXA2 (shEcad/ANXA2). Scale bars: 100 μm.

Annexin A2 is involved in the cancer stemness of lung cancer cells

Annexin A2 is a Ca^{2+}-dependent membrane-binding protein that mediates tumorigenesis and metastasis in non-small cell lung cancer (NSCLC) and is positively correlated with a poor prognosis.[19–21] Here, we found that Annexin A2 expression was upregulated in CSC-like lung cancer cells, and that the CSC-specific aptamer AP-9R recognized CSCs by binding to Annexin A2. To investigate the role of Annexin A2 in cancer stemness, we performed Annexin A2 knockdown in A549^{shEcad} cells with two different lentivirus-based shRNAs targeting Annexin A2 (shANXA2#1 and shANXA2#2), and the effects on the sphere-forming ability, gene expression of stem cell markers, and tumorigenesis were studied. As shown in Figure 3A, Annexin A2 knockdown dramatically suppressed the sphere-forming ability of A549^{shEcad} cells. The gene expression of cancer stemness markers, including Nestin, Nanog, and Oct-4, induced by E-cadherin knockdown was suppressed by simultaneous Annexin A2 knockdown (Figure 3B). Moreover, EMT induced by E-cadherin knockdown was also reversed in A549 cells with double knockdown of E-cadherin and Annexin A2. In A549$^{shEcad/AnxA2}$ cells, expression of the epithelial marker E-cadherin was induced, while expression of the mesenchymal markers Slug and Twist were inhibited (Figure 3C). In addition, the activation of Akt and Erk was suppressed in A549$^{shEcad/AnxA2}$ cells.

Furthermore, we assessed the functional effect of Annexin A2 knockdown on tumorigenesis *in vivo*. A549^{shLuc}, A549^{shEcad}, and A549$^{shEcad/AnxA2}$ cells were subcutaneously injected into NOD/SCID mice. On day 45 after inoculation, the mice were euthanized. As shown in Figure 3D, the volume of tumors derived from A549^{shEcad} cells was larger than that derived from A549^{shLuc} cells, whereas the tumor volume of the A549$^{shEcad/AnxA2}$ cells was reduced. Then, by immunohistochemistry, the expression of Annexin A2, the CSC marker CD44, the proliferation marker Ki67, and the angiogenic marker CD31 were found to be upregulated in A549^{shEcad} tumors compared with A549^{shLuc} tumors, while in A549$^{shEcad/AnxA2}$ tumors, the expression of these genes was downregulated (Figures 3E and S5). In addition, Annexin A2 knockdown reduced the E-cadherin knockdown-increased tumor initiation rate (Table S1). Thus, Annexin A2 knockdown reverses the cancer stem-like properties induced by E-cadherin silencing. In addition to being a CSC antigen, Annexin A2 also plays a functional role in cancer stemness.

AP-9R is a specific molecular probe that effectively captures and recognizes cancer stem-like cells in lung cancer cell lines

Because AP-9R was selected by screening cancer stem-like lung cancer cells, we wanted to investigate the efficacy of CSC capture of AP-9. We used biotin-labeled aptamers and streptavidin magnetic beads to create aptamer-bound beads for the cell capture assay (Figure 4A). First, biotin-labeled AP-9R and biotin-labeled scrambled aptamers (Ap-C) were bound to streptavidin magnetic beads and then

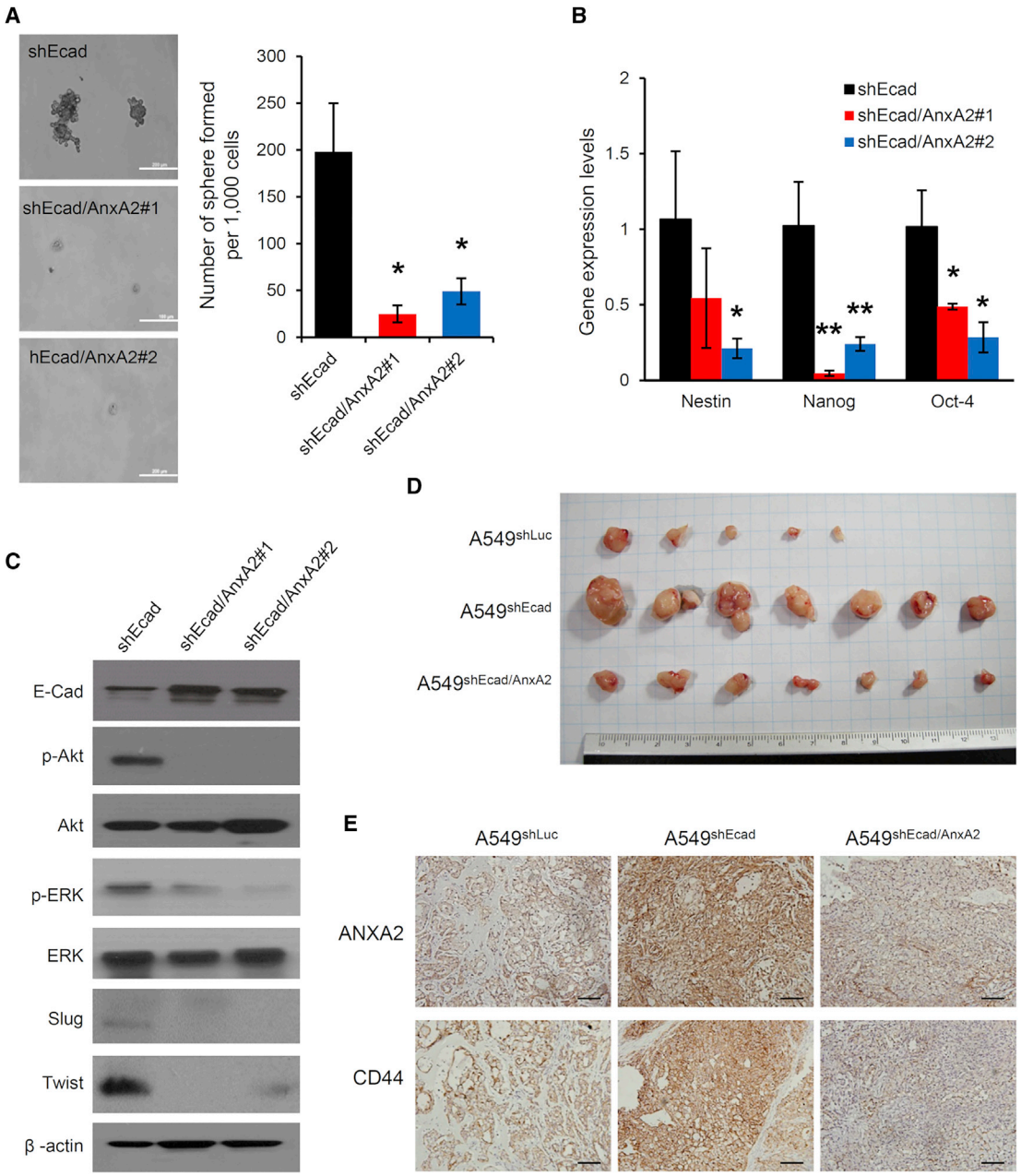

Figure 3. Annexin A2 knockdown reverses the cancer stem-like properties induced by E-cadherin silencing

(A) Annexin A2 knockdown reduces cancer stemness in A549^{shEcad} cells. A549^{shEcad} cells were infected with lentiviruses carrying Annexin A2 shRNAs (shANXA2#1 and shANXA2#2) and then subjected to sphere-forming assays. Scale bars: 200 μm. Error bars show mean ± SD. *$p < 0.05$. (B) Annexin A2 knockdown reduces the expression of cancer stemness markers. The expression of Nestin, Nanog, and Oct-4 in A549^{shEcad} and Annexin A2-knockdown A549^{shEcad} cells (A549$^{shEcad/AnxA2\#1}$ and A549$^{shEcad/AnxA2\#2}$) was examined by qRT-PCR analysis. The error bars show mean ± SD. *$p < 0.05$. **$p < 0.01$. (C) Annexin A2 knockdown reverses EMT. The expression of E-cadherin, Slug, and Twist and the levels of activation of Akt and Erk were analyzed by western blotting with the indicated antibodies. β-Actin was used as the loading control.

(D) Representative images of xenograft tumors from NOD/SCID mice injected with A549 cells infected with shLuc, shEcad, or shEcad plus shANXA2 on day 45 after inoculation. (E) The expression of Annexin A2 (ANXA2) and CD44 in xenograft tumors derived from A549^{shLuc}, A549^{shEcad}, and A549$^{shEcad/AnxA2}$ cells was detected by immunohistochemistry using the indicated antibodies. Scale bars: 200 μm.

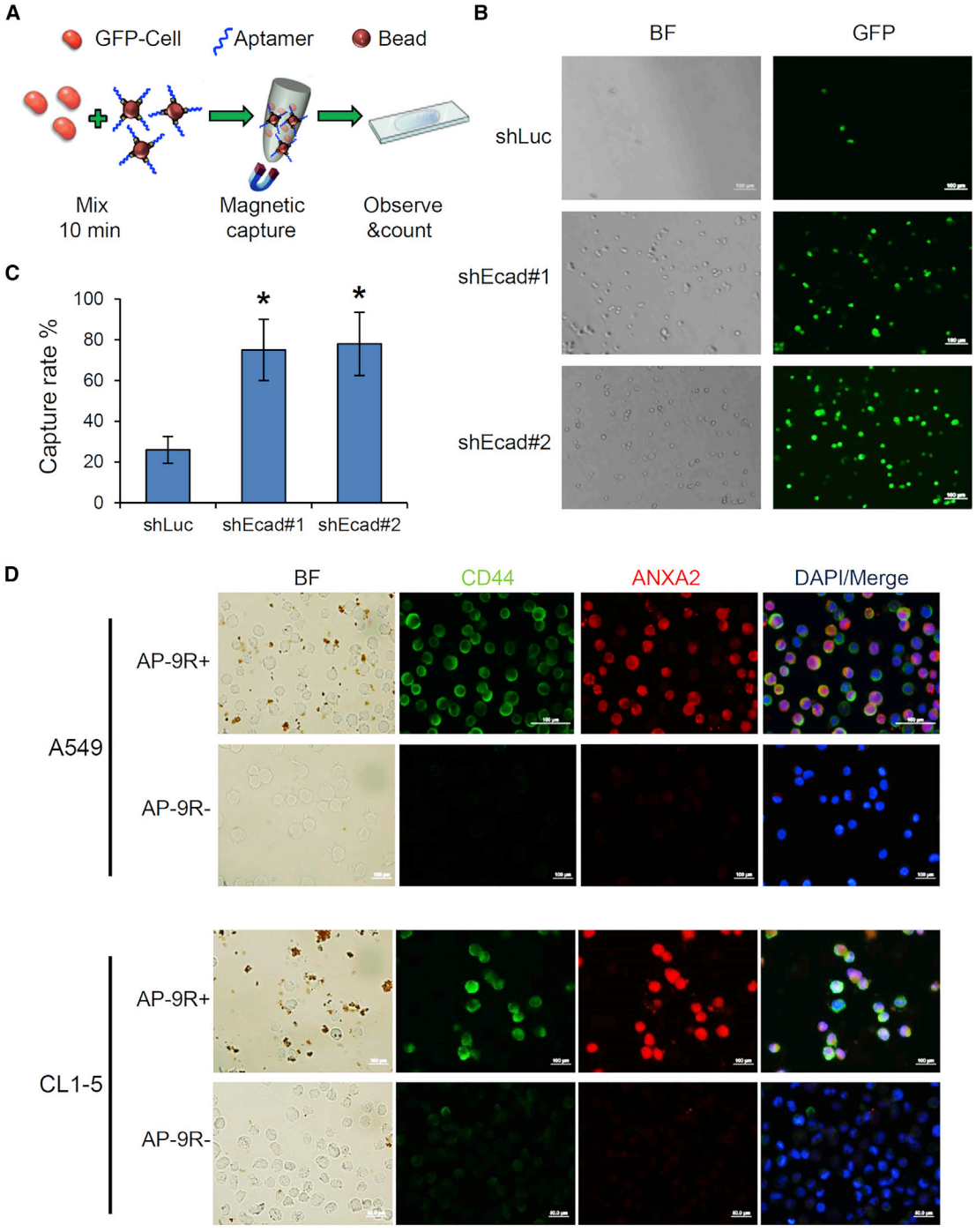

Figure 4. Highly efficient capture of cancer stem-like cells using AP-9R

(A) Schematic of the CSC capture procedure. Biotin-labeled AP-9R was bound to streptavidin magnetic beads, and then the AP-9R-bound beads were incubated with the cells. (B) Representative images of GFP-expressing $A549^{shLuc}$, $A549^{shEcad\#1}$, and $A549^{shEcad\#2}$ cells were captured by AP-9R-bound beads under a fluorescence microscope. Scale bars: 100 μm. (C) The cells captured by the AP-9R-bound beads were counted, and the capture rate was calculated. The error bars show mean ± SD; *$p < 0.05$. (D) Microscopic and immunostaining images of AP-9R-positive ($AP\text{-}9R^{+}$) and AP-9R-negative ($AP\text{-}9R^{-}$) cells enriched from A549 and CL1-5 cells incubated with AP-9R-modified magnetic beads followed by magnetic attraction. CD44 and Annexin A2 are shown in green and red, respectively. Nuclei were visualized by DAPI staining. Scale bars: 50 μm.

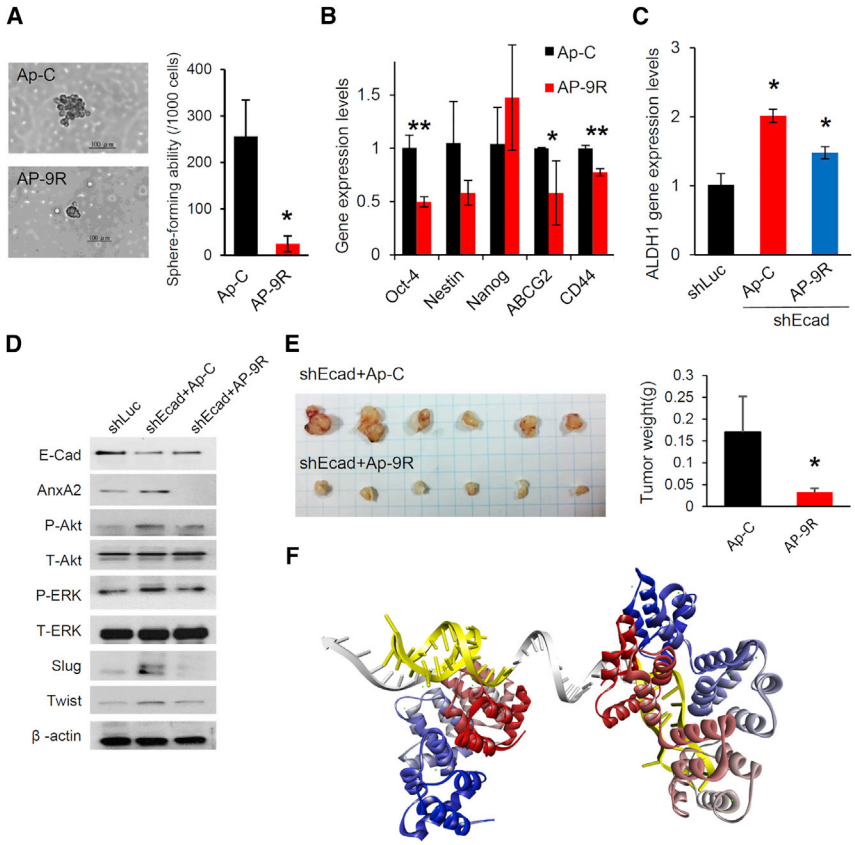

Figure 5. AP-9R inhibits the stem-cell-like properties of lung cancer cells

(A) Left: representative images of spheres formed from A549^{shEcad} cells treated with aptamer control (Ap-C) or AP-9R. Scale bars: 100 μm. Right: the number of spheres (>50 μm in diameter) observed in each well. Data are the mean ± SD. *p < 0.05. (B) qRT-PCR analysis of the expression of Oct-4, Nestin, Nanog, ABCG2, and CD44 in A549^{shEcad} cells treated with aptamer control or AP-9R. GAPDH was used as the internal control. (C) qRT-PCR analysis of ALDH1A1 expression in A549^{shLuc} and A549^{shEcad} cells treated with aptamer control or AP-9R. GAPDH was used as the internal control. The error bars show mean ± SD. *p < 0.05, **p < 0.01. (D) AP-9R suppresses EMT in A549^{shEcad} cells. A549^{shEcad} cells were treated with AP-C or AP-9R. The expression of Annexin A2, E-cadherin, Slug, and Twist and the levels of activation of Akt and Erk were analyzed by western blotting with the indicated antibodies. β-Actin was used as the loading control. (E) Representative images of xenograft tumors from NOD/SCID mice, which were injected with A549^{shEcad} cells and then intratumorally injected with aptamer control or AP-9R, on day 45 after inoculation. The tumor weight was measured. The error bars show mean ± SD. *p < 0.05. (F) The docking simulation of AP-9R (light gray and yellow) with Annexin A2 protein (PDB: 2HYW; from blue to red: N-to-C terminus). In the predicted 3D structure of AP-9R, the arrow and yellow color point to the 3′ terminus of AP-9R and the stem-loop structure of the predicted AP-9R secondary structure, respectively.

incubated with A549^{shEcad} cells. We found that only AP-9R-bound beads interacted with A549^{shEcad} cells, whereas scrambled aptamer-bound beads exhibited nearly no interaction (Figure S6).

Next, we tested GFP-expressing A549^{shLuc}, A549$^{shEcad\#1}$, and A549$^{shEcad\#2}$ cells, as well as AP-9R-bound magnetic beads, to study the efficacy of CSC capture by AP-9. The cells captured by AP-9R were counted under a fluorescence microscope, and then the capture rates of AP-9R for A549^{shLuc}, A549$^{shEcad\#1}$, and A549$^{shEcad\#2}$ cells were calculated. We found that the cell capture rates of AP-9R were approximately 25% for A549^{shLuc} cells and 75–80% for A549^{shEcad} cells (Figures 4B and 4C). These results indicated that AP-9R has a high binding affinity to lung cancer stem-like cells.

Given that AP-9R has a specific affinity for lung cancer stem-like cells, we explored whether AP-9R could be a potential probe to recognize lung cancer stem-like cells in whole cells. As shown in Figure 4D, using AP-9R-bound magnetic beads as probes, AP-9R-positive (AP-9R^{+}) and AP-9R-negative (AP-9R^{-}) cells, meaning cells captured and not captured by AP-9R, respectively, were sorted from A549 and CL1-5 cells. We found that AP-9R + A549 and AP-9R + CL1-5 cells expressed high levels of Annexin A2 and the cancer stem-cell marker CD44 compared with the corresponding AP-9R-cells. These data demonstrate that developing aptamer AP-9R-based technology may lead to novel methods for CSC isolation for the early detection of cancer.

AP-9R inhibits stem-cell-like properties in lung cancer cells

After the successful development of the DNA aptamer for lung cancer stem-like cells, it is very important to assess its cellular functions in CSCs. First, we studied the effect of AP-9R on lung cancer stemness. Compared with the control aptamer (scrambled aptamers), treatment with AP-9R significantly decreased the sphere-forming ability of A549^{shEcad} cells (Figure 5A). Importantly, we found that AP-9R significantly reduced the expression of CSC markers, such as Oct-4, ABCG2, CD44, and ALDH1, in A549^{shEcad} cells (Figures 5B and 5C). Moreover, AP-9R suppressed E-cadherin knockdown-increased cell motility (Figure S7A). AP-9R reduced the levels of Annexin A2 and suppressed E-cadherin knockdown-induced EMT, represented by the upregulation of E-cadherin expression and downregulation of Slug and Twist expression. In addition, upon AP-9R treatment, the levels of phosphorylated Akt and Erk were decreased (Figure 5D).

Furthermore, we assessed the functional effect of AP-9R on tumorigenesis *in vivo*. A549^{shEcad} cells were subcutaneously injected into NOD/SCID mice, and then the control aptamer or AP-9R was injected into the tumors. On day 45 after inoculation, the mice were euthanized. As shown in Figure 5E, AP-9R dramatically reduced

the tumor weight, although AP-9R had no effect on the proliferation of A549^{shLuc} and A549^{shEcad} cells *in vitro* (Figure S7B).

In addition, we used the PatchDock Server[22] (http://bioinfo3d.cs.tau.ac.il/PatchDock/), which is a molecular docking algorithm based on shape complementarity principles, to resolve the interaction of AP-9R and Annexin A2. Because of the lack of ssDNA 3D structure prediction software, the AP-9R structure was predicted to be an RNA aptamer by modeling and using RNAcomposer (http://rnacomposer.cs.put.poznan.pl/) for 3D structure prediction. According to the docking results of AP-9R and Annexin A2 protein (PDB: 2HYW), the interaction structure with the lowest free energy was shown in Figure 5F, and AP-9R might interact with Annexin A2 via two stem-loop structures, binding to the respective structures of Annexin A2 protein. Taken together, AP-9R, by targeting Annexin A2, suppresses cancer stemness, EMT, and tumorigenesis in lung cancer stem-like cells.

Annexin A2 expression is associated with stemness, EMT, metastasis signature, and poor clinical outcomes in lung cancer

Based on the above results, we demonstrated a critical role of Annexin A2 (*ANXA2*) in regulating lung cancer stemness, and targeting Annexin A2 with shRNA or aptamer reverses EMT and decreases cell motility and CSC-like properties. However, the clinical relevance of Annexin A2 in lung cancer remains poorly understood. To investigate the relationship between Annexin A2 and stemness-related signatures in lung cancer, we performed GSEA of the TCGA-LUAD cohort (n = 517).[16] The GSEA results showed that high *ANXA2* expression was positively correlated with stem cell signatures in the TCGA-LUAD dataset (Figure 6A). We further found that *ANXA2* expression was positively correlated with cell migration and metastasis signatures in the TCGA-LUAD dataset as well (Figures 6B and 6C). Consistent with this finding, we also observed that *ANXA2* expression was positively correlated with expression of the stem cell marker *CD44* in TCGA lung squamous cell carcinoma (TCGA-LUSC; n = 502) and TCGA-LUAD datasets (Figure 6D). Moreover, increasing amounts of evidence have linked EMT to the acquisition of stem cell properties, and CSCs play a critical role in tumor metastasis in several cancers.[14,23] In addition, *ANXA2* expression was elevated in tumors with lymph node metastasis compared with those without metastasis (Figure 6E).

Furthermore, we investigated the association between *AXNA2* and survival in lung cancer. By analyzing the TCGA dataset and the online Kaplan-Meier plotter database,[24] we found that lung cancer patients with higher *AXNA2*-expressing tumors were associated with poor overall survival regardless of whether they were adenocarcinoma or squamous cell carcinoma (Figure 6F). Taken together, Annexin A2 correlates with CSCs and metastasis of lung cancer and may be a biomarker for predicting the survival of lung cancer patients.

DISCUSSION

Although breakthrough improvements in cancer treatment have recently occurred, patients still die of cancer. CSCs are recognized as the underlying reason because of their properties of tumor recurrence, drug resistance, and metastasis promotion. Here, we used cancer stem-like A549^{shEcad} cells and cell-SELEX screening to identify a novel CSC-targeting aptamer, AP-9R. The target of AP-9R was identified to be Annexin A2, which is involved in cancer stemness, tumor growth, and cancer cell motility, and whose expression is correlated with poor survival of lung cancer patients. Furthermore, AP-9R could not only recognize CSCs but also suppress cancer stemness, tumor growth, and the motility of cancer stem-like cells. AP-9R may function as both a detector and a therapeutic agent for CSC targeting.

The tumor mass consists of bulk tumor cells and a rare subpopulation (<1%) of CSCs within the bulk tumor cells.[25] Current cancer therapeutic strategies usually kill the bulk tumor cells, but not the CSCs, resulting in disease recurrence or cancer metastasis. Therefore, targeting CSCs may provide an opportunity to cure cancer. Recent studies have explored six pathways that confer cancer stemness, such as the Hedgehog, Notch, Nanog, JAK/STAT, phosphatidylinositol 3-kinase (PI3K)/Akt, and Wnt/β-catenin pathways, and several CSC biomarkers in various cancers, but these pathways and biomarkers are not universal or uniform among different cancer types.[26,27] Currently, small molecules targeting CSCs are usually developed by inhibiting one of the six pathways, although none has been promoted as a CSC-targeting agent. For example, two approved Hedgehog inhibitors, vismodegib and sonidegib, antagonize the Smoothened (SMO) protein to inhibit various cancers and CSC characteristics,[28] while another approved agent, duvelisib, a PI3K inhibitor, also reduces CSC properties in lymphoma in addition to its antitumor effect.[29] Moreover, among the CSC markers, CD44 and CD133 are the most common surface markers reported in different cancers. Antibodies and aptamers targeting CD44 or CD133 have been developed and designed as drug delivery systems for cancer therapy.[30,31] In addition, targeting CD44 itself could effectively block tumor growth, metastasis, recurrence, and drug resistance. However, because of the many splice variants and posttranslational modifications of CD44 and CD133, the currently available antibodies are limited in their ability to effectively detect these molecules, resulting in little progress in therapeutic development. Therefore, the discovery of novel molecules for targeting CSCs is extremely useful for the treatment and diagnosis of advanced malignancy. Fortunately, in this study, by cell-SELEX, we identified a novel CSC-targeting aptamer, AP-9R, which specifically bound and antagonized Annexin A2. Then, we showed that Annexin A2 is involved in EMT and cancer stemness. Moreover, activation of the Akt and Erk pathways was documented in breast CSCs.[32] Similarly, we found that E-cadherin knockdown (causing cancer stem-like properties) also increased the levels of phosphorylated Akt and Erk, whereas Annexin A2 knockdown and AP-9R blocked these effects. Taken together, we suggest that AP-9R may serve as a novel detector and inhibitor of CSCs, and that its target, Annexin A2, may be a novel target for CSC therapy.

Recent studies have described DNA or RNA aptamers that specifically recognize small molecules, toxins, linear epitopes (peptides), and conformational epitopes of target proteins, pathogens, or cells with high affinity.[10,33,34] Due to their unique characteristics, including

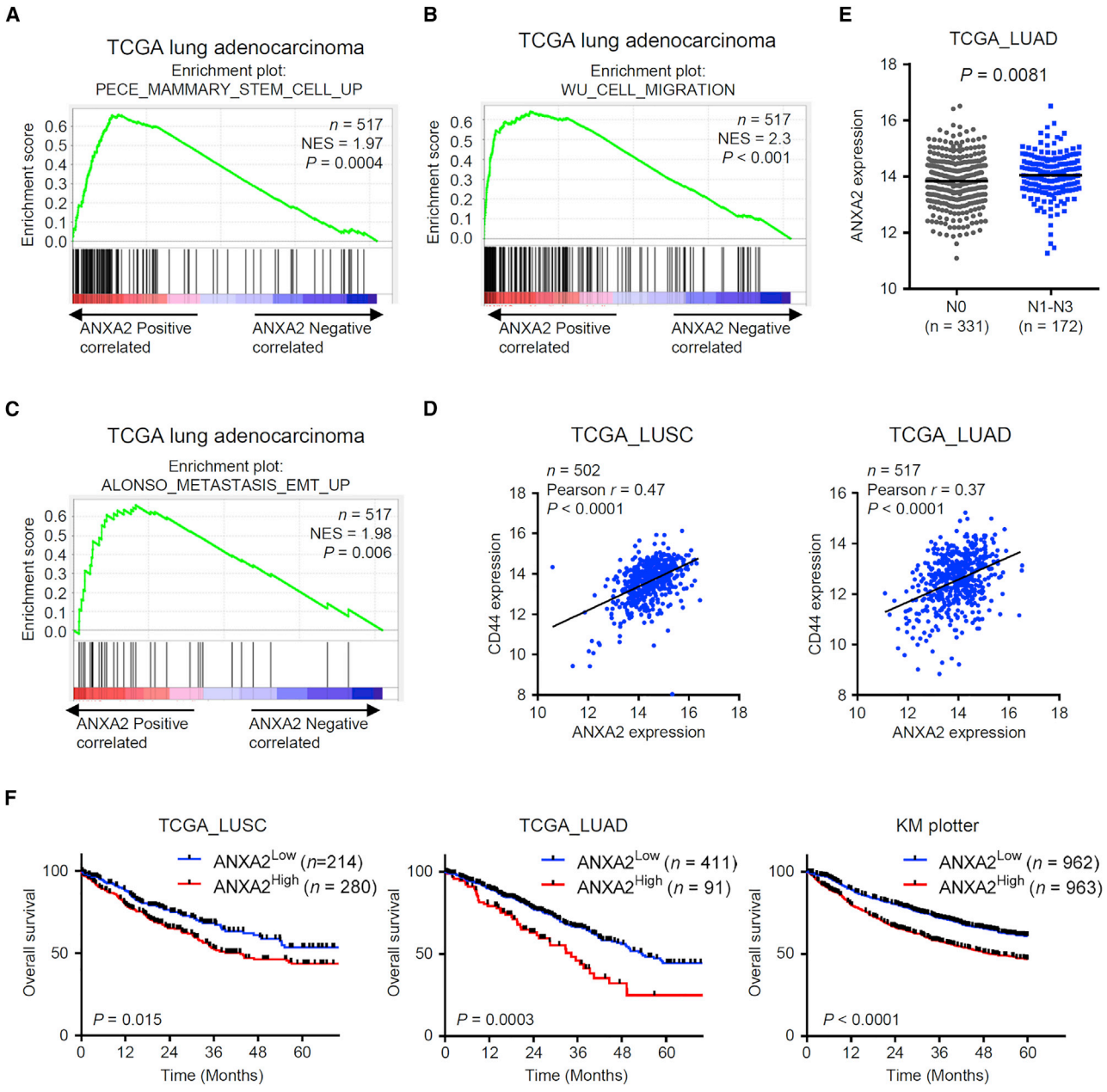

Figure 6. *ANXA2* expression is correlated with stemness, metastasis-related signatures, and poor clinical outcomes in lung cancer

(A–C) Enrichment plots of gene expression signatures for stem cell (A), EMT-metastasis (B), and cell migration-related pathways (C) according to the *ANXA2* expression levels. The barcode plot indicates the positions of the genes in each gene set; red and blue colors represent positive and negative Pearson correlations with *ANXA2* expression, respectively. (D) Correlation between *ANXA2* and *CD44* expression in TCGA-LUSC and TCGA-LUAD datasets, determined using Pearson's correlation analysis. (E) Expression of *AXNA2* in patients with lymph node metastasis (N1–N3) compared with the patients without metastasis (N0) using the TCGA-LUAD dataset. The p values were calculated by Student's t test. (F) Kaplan-Meier (KM) analysis showing that high expression of *ANXA2* is significantly associated with worse overall survival in the TCGA-LUSC, TCGA-LUAD, and KM plotter datasets. p values were based on the log rank test. NES, normalized enrichment score.

high specificity, affinity, and stability in different environments, low immunogenicity and toxicity, ease of synthesis and chemical modification/conjugation with functional groups, siRNA, drug nanoparticles, or imaging agents, and ease of penetration into cells, aptamers are preferentially being used in diagnostic and therapeutic areas instead of antibodies.[8–10] Currently, a 27-mer RNA aptamer, pegaptanib (Macugen), targeting vascular endothelial growth factor (VEGF) has been approved by the US Food and Drug Administration

(FDA). Recently, several aptamers have been developed to recognize cancer cells.[10–13] Here, we found that whole-cell SELEX, focusing on a cancer stem-like cell phenotype, could yield ligands able to disrupt key functions of particular importance for cancer progression. In this study, we used lung cancer stem-like cells ($A549^{shEcad}$) as the target cell line and noncancer stem-like cells ($A549^{shLuc}$) as the control cell line, and all the selections were performed in culture dishes. We believe this system is an accurate representation of the native state of the surface markers in CSCs. Using our cell-based SELEX strategy, we discovered a DNA aptamer, AP-9R. AP-9R showed high specificity and affinity for the surface target on most lung cancer stem-like cells, but not noncancer stem-like cells or the normal lung epithelial cell line BEAS2B. AP-9R itself showed no inherent cytotoxicity to either control or target cells. In addition, in the presence of AP-9R, the migration ability, cancer stemness, and tumorigenesis of cancer stem-like cells were inhibited. These data support the development of AP-9R as a potential diagnostic and therapeutic agent for CSCs.

Herein, we identified Annexin A2 as the target of AP-9R and characterized the role of Annexin A2 in CSC properties. Annexin A2 belongs to the highly conserved Annexin family, which contains 13 members in vertebrates and is a Ca^{2+}-regulated phospholipid-binding protein.[35] Among annexins, Annexin A2 is reported to be overexpressed or to predict a poor prognosis in a variety of cancers, including NSCLC, breast cancer, ovarian cancer, gastric cancer, hepatocellular carcinoma, pancreatic cancer, colorectal carcinoma, cholangiocarcinoma, glioblastoma, nasopharyngeal carcinoma, and multiple myeloma, but not prostate cancer or oral squamous cell carcinoma.[36] Annexin A2 has multiple functions that can promote cancer progression. Nuclear Annexin A2 is involved in DNA synthesis by stimulating DNA polymerase α. Moreover, in the cytosol or on the cell surface, Annexin A2 binds to the inner or outer leaflet of the membrane and forms a heterotetramer with S100A10, binds to Ca^{2+} or interacting proteins via its C-terminal domain, and interacts with F-actin and phospholipids via its N-terminal domain. Annexin A2 is involved in cytokinesis, endocytosis, exocytosis, signal transduction, and biochemical activation of plasminogen to plasmin. All of these roles promote cancer cell proliferation, extracellular matrix degradation, cancer cell migration and invasion, metastasis, and neoangiogenesis.[36] Not surprisingly, anti-Annexin A2 neutralizing antibodies or shRNAs targeting Annexin A2 were reported to suppress tumor growth, neoangiogenesis, and metastasis. In addition, Annexin A2 also contributes to cisplatin resistance in A549 cells[37] and gemcitabine resistance in pancreatic cancer cells.[38] Circulating levels of Annexin A2 can predict chemotherapy resistance in gastric cancer and can also be found in patients with breast cancer or hepatocellular carcinoma.[36] Taken together, although Annexin A2 has been reported to play multifunctional roles in cancer progression and chemoresistance, the role of Annexin A2 in CSCs has not been specifically addressed. In this study, we found that Annexin A2 was highly expressed in lung CSCs isolated by either AP-9R capture, $ALDH^+$ sorting, or Hoechst SP, and Annexin A2 knockdown suppressed cancer stemness, including the expression of cancer stemness markers, sphere formation ability, and TIC frequency. Moreover, Annexin A2 knockdown also suppressed EMT, tumorigenesis of CSCs, and angiogenesis. In the clinic, Annexin A2 expression was correlated with signatures of stemness, cell migration, and EMT/metastasis in TCGA-LUAD. We addressed the role of Annexin A2 in lung cancer stemness and the therapeutic potential of Annexin A2 inhibition by shRNA or AP-9R in lung cancer.

Collectively, we identified a CSC-targeting DNA aptamer, AP-9R, that specifically binds and neutralizes Annexin A2 on the cell surface to suppress tumorigenesis, cancer progression, and angiogenesis in lung cancer. Although DNA-based aptamers are small, synthetic targeting agents, they still must overcome several obstacles before being used successfully as therapeutic agents. Nevertheless, AP-9R provides a simple scaffold for developing DNA-based biomarkers or inhibitors for lung CSCs and other Annexin A2-upregulated cancers, although additional studies may be necessary to determine their diagnostic and prognostic significance in clinical studies.

MATERIALS AND METHODS

Cell lines

The human lung adenocarcinoma A549 cells were cultured in Dulbecco's modified Eagle's medium (DMEM) containing 10% fetal bovine serum (FBS) and antibiotics. The human non-tumorigenic lung epithelial cell line BEAS-2B and human lung adenocarcinoma CL1-5 were cultured in RPMI 1640 supplemented with 10% FBS and antibiotics. CL1-5 was established in our laboratory.[39] A549 and BEAS-2B were obtained from the American Type Culture Collection (ATCC, Manassas, VA, USA). All cell lines were cultured at 37°C under a humidified atmosphere consisting of 5% CO_2.

Lentivirus production and infection

The shRNAs targeting E-cadherin, Annexin A2, and luciferase were obtained from the National RNAi Core Facility located at the Institute of Molecular Biology/Genomic Research Center, Academia Sinica, Taiwan. After HEK293T cells were cotransfected with pLKO.1shRNA, pCMV △R8.91, and pMD.G for 24 and 48 h, virus-containing medium was collected. Viral titers were determined by transmuting HEK293T cells using diluted culture supernatants and tested by counting the number of viable cells after 2 days of culture in the presence or absence of antibiotics. Viral supernatants were stored at −80°C. Cells were infected with lentiviruses in the presence of 8 μg/mL polybrene (Sigma-Aldrich, St. Louis, MO, USA). After 24 h-infection, the cells were treated with puromycin to select for a pool of puromycin-resistant clones used for subsequent analysis.

Library preparation and reagents for SELEX

The DNA library was synthesized and purified by Medclub Scientific, Taiwan. Each DNA sequence of the library contains a central random region of 40 bases flanked by two specific 16-base sequences that function as primer-binding sites (5′-GGCAGGAAGACAAACA-N40-GGTCTGTGGTGCTGT-3′) for subsequent PCR process. Here, we used lung cancer stem-like cells ($A549^{shEcd}$) as the target cell line and non-cancer stem like cells ($A549^{shLuc}$) as the control cell line for negative selection, and all selections were performed in

the culture dish. In the first round of positive selection, 100 pmol ssDNA library was incubated with $A549^{shEcad}$ cells at 4°C for 30 min. After unbound ssDNAs were washed out from target cells, the bound ssDNAs were eluted by heating at 95°C for 5 min and then incubated with control cells ($A549^{shLuc}$) at 4°C for another 30 min. Following that, unbound ssDNA pools from control cells were amplified by PCR to start the next cycle. A washing buffer containing 1 L of Dulbecco's phosphate-buffered saline (DPBS), 4.5 g of glucose, and 5 mL of 1 M $MgCl_2$ was stored at 4°C for up to 3 months. The binding buffer containing 1 L of DPBS, 4.5 g of glucose, 100 mg of tRNA, 1 g of bovine serum albumin (BSA), and 5 mL of 1 M $MgCl_2$ was stored at 4°C for up to 1 month. Every round used 3 mL of washing buffer for the washing process and 1 mL of binding buffer for incubation. PCR reagents contained 0.5 μM forward primers (5′-GGCAGGAAGACAAACA-3′), 0.5 μM reverse primers (5′-AC AGCACCACAGACCA-3′), 1.5 mM $MgCl_2$, 0.2 mM deoxynucleotide triphosphates (dNTPs), and 2 U Super-Therm Gold DNA polymerase (Bertec Enterprise, Taiwan). The PCR process was started with an initial denaturing at 94°C for 10 min, followed by 20 cycles of denaturation at 94°C for 30 s, annealing at 60°C for 15 s, and extension at 72°C for 30 s. A final extension step at 72°C for 7 min was carried out following the last cycle. After a successful 15-round selection, the enriched pool of ssDNAs was amplified by PCR, and the PCR products were purified and cloned using the yT&A cloning kit (Sigma-Aldrich) for identification of the CSC-specific aptamers. Ten colonies were randomly selected and purified.

Aptamer binding assay

Cells were seeded (1×10^4) into 24-well plates and treated with 100 nM ssDNA pool (scrambled aptamers) or AP-9R at 4°C for 30 min. Then cells were washed by PBS and lysed at 95°C for 5 min. Aptamers were amplified by PCR.

Flow cytometric analysis

The binding affinity of the aptamers was determined by incubation of target cells (5×10^5) for 10 min on ice with varying concentrations of 5′-FAM-labeled AP-9R in 200 μL of binding buffer in the dark. Cells were then washed twice with 1 mL of the washing buffer, suspended in 0.4 mL of binding buffer, and subjected to flow cytometry analysis. The fluorescence was determined with a FACScan cytometer (BD Biosciences, San Jose, CA, USA). All of these experiments were repeated two times.

Immunofluorescence staining

For confocal imaging, cells (1×10^3) were seeded onto poly-L-lysine-coated glass coverslips in 24-well dishes. After 24 h, cells were treated with 100 nM 6′-FAM-labeled AP-9R at 4°C for 30 min, then washed twice with washing buffer and subsequently fixed in PBS with 4% formaldehyde. Cell nuclei were stained by 4',6-diamidino-2-phenylindole (DAPI). Imaging of the control and target cells was performed with a confocal microscope under visible light and 488 nm excitation light. For immunofluorescence staining, cells were fixed in PBS with 4% formaldehyde, permeabilized in PBS containing 0.5% Triton X-100, and blocked in PBS with 1% BSA. Then cells were incubated with an anti-Annexin A2 (GeneTex, San Antonio, TX, USA) or anti-CD44 (ab112178; Abcam, Cambridge, MA, USA) antibody diluted 1:100 in blocking solution. The cells were washed and incubated with Fluorescein (FITC)- or Tetramethylrhodamine (TRITC)-conjugated secondary antibody (Jackson ImmunoResearch Lab, West Grove, PA, USA). Nuclei were demarcated with DAPI staining. The cells on coverslips were mounted onto slides and visualized using fluorescence microscopy.

Quantitative RT-PCR (qRT-PCR)

Total cell RNA was isolated using TRIzol Reagent (Invitrogen, Eugene, OR, USA) and reverse transcribed to complementary DNA (cDNA) using a mirVana qRT-PCR miRNA Detection Kit (Applied Biosystems/Ambion, Foster City, CA, USA) or ImProm-II Reverse Transcriptase (Promega, San Luis Obispo, CA, USA) according to the manufacturer's instructions. qRT-PCR was carried out using a LightCycler 480 Instrument (Roche Applied Sciences, Mannheim, Germany) and SYBR Green I dye (Roche Applied Sciences). GAPDH was used as an internal control for mRNA quantification. All reactions were performed in triplicate.

Western blotting

The protein lysate was subjected to SDS-PAGE and transferred to a polyvinylidene fluoride (PVDF) membrane. Protein expression was analyzed by western blotting using primary antibodies against E-cadherin (Clone 36B5; NeoMarkers, Fremont, CA, USA), Vimentin (C-20; Santa Cruz Biotechnology, Santa Cruz, CA, USA), Slug (Santa Cruz Biotechnology), Twist (GeneTex), Annexin A2 (GeneTex), phosphorylated and total Akt (Cell Signaling Technology, Beverly, MA, USA), phosphorylated and total Erk (Cell Signaling Technology), or β-actin (Sigma-Aldrich), followed by incubation with horseradish peroxidase-conjugated secondary antibodies. Specific proteins were detected by chemiluminescence using ECL Plus Western Blotting Detection Reagents (GE Healthcare Biosciences, Piscataway, NJ, USA).

Identification of the protein target of AP-9R

A membrane extract of $A549^{shEcad}$ cells was prepared using a Membrane-Cytosol extraction kit (Calbiochem, San Diego, CA, USA). The membrane protein lysate was incubated with 0.1 μM biotin-labeled AP-9R and Streptavidin-conjugated M-PVA Magnetic Beads (Chemagen, Chemagic, Germany). Then the pull-down complex was subjected to 12% SDS-PAGE and stained with Coomassie Brilliant Blue R-250. The protein bands of interest were excised, subjected to in-gel tryptic digestion, and analyzed by mass spectrometry-based proteomics as described in the supplemental materials and methods.

Pull-down assay

Cell lysate (0.5 mg) from $A549^{shEad}$ cells was incubated with biotin-labeled AP-9R (0.1 μM) in 500 μL of the binding/wash buffer (20 mM HEPES [pH 7.4], 100 mM KCl, and 2 mM 2-mercaptoethanol) with 0.5% Tween 20 for 12 h at 4°C. Then the supernatant was mixed with 50 μL of Streptavidin-M-PVA Magnetic Beads (Chemagen). After incubation for 6 h at 4°C, the beads were isolated and

washed with the binding/wash buffer containing 0.1% Tween 20. The bound proteins were eluted with SDS sample buffer. The eluted proteins were separated on a 12% SDS-PAGE gel and visualized by immunoblot analysis with the monoclonal anti-Annexin A2 antibody.

Sphere formation assay

To assay sphere formation, we plated 1×10^3 cells onto a six-well ultra-low attachment plate (Corning Glass) in serum-free DMEM supplemented with N-2 supplement, 10 ng/mL epidermal growth factor (EGF), and 10 ng/mL basic fibroblast growth factor (bFGF) (Invitrogen). After 14 days of culture, the number of tumor spheres formed at least 50 μm in diameter was counted using an inverted microscope.

Tumorigenic assay in NOD/SCID mice

All experiments were carried out using male 6-week-old NOD/SCID mice. A total of 1×10^3 cells were re-suspended in PBS and mixed with Matrigel (BD Biosciences) at a 1:1 ratio and subcutaneously injected into the right flank of NOD/SCID mice. Tumor size was measured with calipers using the formula: $V = ab^2/2$, where a is the length and b is the width of the tumor. When tumors were palpable, NOD/SCID mice were intratumorally injected Ap-C or AP-9R (1 mg/kg in 50 μL) three times a week. On day 45, the primary tumors were excised and weighed. The tissue specimens were fixed in 10% buffered formalin and embedded in paraffin and sectioned.

Immunohistochemistry

The paraffin sections were first autoclaved in citrate buffer (pH 6.0) at 121°C for 10 min. Then sections were treated with 3% H_2O_2 and incubated with anti-Annexin A2, anti-CD44, anti-Ki-67 (550609; BD Biosciences), or anti-CD31 (ab9498; Abcam) antibodies diluted in antibody diluent (Biocare Medical, Concord, CA, USA) for 4°C overnight. After washing by PBS, the sections were allowed to react with the HRP-conjugated secondary antibodies, incubated with AEC chromogen (Dako, Carpinteria, CA, USA), and then counterstained with hematoxylin.

Capture assay

Biotin-labeled AP-9R was incubated with Streptavidin-M-PVA Magnetic Beads in PBS at 4°C for 3 h. The AP-9R-bound beads were incubated with GFP-labeled cells (1×10^4). After 30-min incubation, the capture rates were calculated as follows: Capture rate = captured cancer cells/total number of cancer cells × 100%.

Clinical analysis of ANXA2 in lung cancer

In order to explore biological processes related with *ANXA2* expression, we conducted GSEA[40] using C2 curated gene sets from the molecular signatures database (MSigDB). RNA-seq data from TCGA-LUAD were imported into the GSEA program. GSEA was conducted with 1,000 phenotype permutations using a continuous increasing phenotype label based on *ANXA2* expression. The metric for ranking genes was set as 'Pearson.' To examine the clinical relevance of *ANXA2* expression in lung cancer, we downloaded expression profiles and clinical data from the TCGA-LUAD and TCGA-LUSC cohorts by the University of California Santa Cruz (UCSC) Xena browser (https://xenabrowser.net/).[41] The optimal cut point for *ANXA2* expression was determined by using X-tile software version 3.6.1.[42] In addition, the prognostic significance of *ANXA2* expression in lung cancer was also assessed by the Kaplan-Meier plotter online database (https://www.kmplot.com).[43]

SUPPLEMENTAL INFORMATION

Supplemental information can be found online at https://doi.org/10.1016/j.omtn.2022.01.012.

ACKNOWLEDGMENTS

We are grateful for the services provided by the Immunobiology Core and the RNAi Core Lab, Clinical Medicine Research Center, National Cheng Kung University Hospital, Taiwan. RNAi reagents were obtained from the National RNAi Core Facility located at the Institute of Molecular Biology/Genomic Research Center, Academia Sinica, Taiwan. This study was supported by grants MOST 102-2314-B-006-024-MY3, 109-2314-B-006-057-MY3, and 110-2314-B-006-073-MY3 from the Ministry of Science and Technology, Taiwan.

AUTHOR CONTRIBUTIONS

Y.-Y.W. and I.-S.H. wrote the manuscript, performed the majority of the experiments, and analyzed the data. C.-H.T. analyzed the *in silico* data. C.-H.W., J.-E.W., and J.-S.Y. helped to perform the experiments and analyze the data. T.-M.H. and Y.-L.C. supervised the study and revised the manuscript.

DECLARATION OF INTERESTS

The authors declare no competing interests.

REFERENCES

1. Lobo, N.A., Shimono, Y., Qian, D., and Clarke, M.F. (2007). The biology of cancer stem cells. Annu. Rev. Cell. Dev. Biol. *23*, 675–699.
2. Gupta, P.B., Onder, T.T., Jiang, G., Tao, K., Kuperwasser, C., Weinberg, R.A., and Lander, E.S. (2009). Identification of selective inhibitors of cancer stem cells by high-throughput screening. Cell *138*, 645–659.
3. Klonisch, T., Wiechec, E., Hombach-Klonisch, S., Ande, S.R., Wesselborg, S., Schulze-Osthoff, K., and Los, M. (2008). Cancer stem cell markers in common cancers - therapeutic implications. Trends. Mol. Med. *14*, 450–460.
4. Zhou, B.B., Zhang, H., Damelin, M., Geles, K.G., Grindley, J.C., and Dirks, P.B. (2009). Tumour-initiating cells: challenges and opportunities for anticancer drug discovery. Nat. Rev. Drug Discov. *8*, 806–823.
5. Famulok, M., Hartig, J.S., and Mayer, G. (2007). Functional aptamers and aptazymes in biotechnology, diagnostics, and therapy. Chem. Rev. *107*, 3715–3743.
6. Tan, W., Wang, H., Chen, Y., Zhang, X., Zhu, H., Yang, C., Yang, R., and Liu, C. (2011). Molecular aptamers for drug delivery. Trends. Biotechnol. *29*, 634–640.
7. Yang, X., Li, N., and Gorenstein, D.G. (2011). Strategies for the discovery of therapeutic aptamers. Expert Opin. Drug Discov. *6*, 75–87.
8. Esposito, C.L., Passaro, D., Longobardo, I., Condorelli, G., Marotta, P., Affuso, A., de Franciscis, V., and Cerchia, L. (2011). A neutralizing RNA aptamer against EGFR causes selective apoptotic cell death. PLoS One *6*, e24071.
9. Ireson, C.R., and Kelland, L.R. (2006). Discovery and development of anticancer aptamers. Mol. Cancer Ther. *5*, 2957–2962.
10. Kumar Kulabhusan, P., Hussain, B., and Yuce, M. (2020). Current perspectives on aptamers as diagnostic tools and therapeutic agents. Pharmaceutics *12*, 646.

11. Cerchia, L., and de Franciscis, V. (2010). Targeting cancer cells with nucleic acid aptamers. Trends. Biotechnol. *28*, 517–525.
12. Sefah, K., Meng, L., Lopez-Colon, D., Jimenez, E., Liu, C., and Tan, W. (2010). DNA aptamers as molecular probes for colorectal cancer study. PLoS One *5*, e14269.
13. Van Simaeys, D., Lopez-Colon, D., Sefah, K., Sutphen, R., Jimenez, E., and Tan, W. (2010). Study of the molecular recognition of aptamers selected through ovarian cancer cell-SELEX. PLoS One *5*, e13770.
14. Wang, H., and Unternaehrer, J.J. (2019). Epithelial-mesenchymal transition and cancer stem cells: at the crossroads of differentiation and dedifferentiation. Dev. Dyn. *248*, 10–20.
15. Wilson, M.M., Weinberg, R.A., Lees, J.A., and Guen, V.J. (2020). Emerging mechanisms by which EMT programs control stemness. Trends. Cancer *6*, 775–780.
16. Deng, M., Bragelmann, J., Schultze, J.L., and Perner, S. (2016). Web-TCGA: an online platform for integrated analysis of molecular cancer data sets. BMC Bioinformatics *17*, 72.
17. Huang, B.T., Lai, W.Y., Chang, Y.C., Wang, J.W., Yeh, S.D., Lin, E.P., and Yang, P.C. (2017). A CTLA-4 antagonizing DNA aptamer with antitumor effect. Mol. Ther. Nucleic Acids *8*, 520–528.
18. Weng, C.-H., Hsieh, I.S., Hung, L.-Y., Lin, H.-I., Shiesh, S.-C., Chen, Y.-L., and Lee, G.-B. (2013). An automatic microfluidic system for rapid screening of cancer stem-like cell-specific aptamers. Microfluid. Nanofluidics *14*, 753–765.
19. Sharma, M.C., and Sharma, M. (2007). The role of annexin II in angiogenesis and tumor progression: a potential therapeutic target. Curr. Pharm. Des. *13*, 3568–3575.
20. Wang, C.Y., Chen, C.L., Tseng, Y.L., Fang, Y.T., Lin, Y.S., Su, W.C., Chen, C.C., Chang, K.C., Wang, Y.C., and Lin, C.F. (2012). Annexin A2 silencing induces G2 arrest of non-small cell lung cancer cells through p53-dependent and -independent mechanisms. J. Biol. Chem. *287*, 32512–32524.
21. Zhai, H., Acharya, S., Gravanis, I., Mehmood, S., Seidman, R.J., Shroyer, K.R., Hajjar, K.A., and Tsirka, S.E. (2011). Annexin A2 promotes glioma cell invasion and tumor progression. J. Neurosci. *31*, 14346–14360.
22. Schneidman-Duhovny, D., Inbar, Y., Nussinov, R., and Wolfson, H.J. (2005). PatchDock and SymmDock: servers for rigid and symmetric docking. Nucleic Acids Res. *33*, W363–W367.
23. Lu, W., and Kang, Y. (2019). Epithelial-mesenchymal plasticity in cancer progression and metastasis. Dev. Cell *49*, 361–374.
24. Gyorffy, B., Lanczky, A., Eklund, A.C., Denkert, C., Budczies, J., Li, Q., and Szallasi, Z. (2010). An online survival analysis tool to rapidly assess the effect of 22,277 genes on breast cancer prognosis using microarray data of 1,809 patients. Breast Cancer Res. Treat *123*, 725–731.
25. Bao, B., Ahmad, A., Azmi, A.S., Ali, S., and Sarkar, F.H. (2013). Overview of cancer stem cells (CSCs) and mechanisms of their regulation: implications for cancer therapy. Curr. Protoc. Pharmacol. *Chapter 14*, Unit 14 25.
26. Visvader, J.E., and Lindeman, G.J. (2012). Cancer stem cells: current status and evolving complexities. Cell Stem Cell *10*, 717–728.
27. Lathia, J., Liu, H., and Matei, D. (2020). The clinical impact of cancer stem cells. Oncologist *25*, 123–131.
28. Jeng, K.S., Sheen, I.S., Leu, C.M., Tseng, P.H., and Chang, C.F. (2020). The role of smoothened in cancer. Int. J. Mol. Sci. *21*, 6863.
29. Chen, J., Ge, X., Zhang, W., Ding, P., Du, Y., Wang, Q., Li, L., Fang, L., Sun, Y., Zhang, P., et al. (2020). PI3K/AKT inhibition reverses R-CHOP resistance by destabilizing SOX2 in diffuse large B cell lymphoma. Theranostics *10*, 3151–3163.
30. Chen, C., Zhao, S., Karnad, A., and Freeman, J.W. (2018). The biology and role of CD44 in cancer progression: therapeutic implications. J. Hematol. Oncol. *11*, 64.
31. Glumac, P.M., and LeBeau, A.M. (2018). The role of CD133 in cancer: a concise review. Clin. Transl. Med. *7*, 18.
32. Wang, Y.K., Zhu, Y.L., Qiu, F.M., Zhang, T., Chen, Z.G., Zheng, S., and Huang, J. (2010). Activation of Akt and MAPK pathways enhances the tumorigenicity of CD133+ primary colon cancer cells. Carcinogenesis *31*, 1376–1380.
33. Morris, K.N., Jensen, K.B., Julin, C.M., Weil, M., and Gold, L. (1998). High affinity ligands from in vitro selection: complex targets. Proc. Natl. Acad. Sci. U S A *95*, 2902–2907.
34. Shin, S., Kim, I.H., Kang, W., Yang, J.K., and Hah, S.S. (2010). An alternative to Western blot analysis using RNA aptamer-functionalized quantum dots. Bioorg. Med. Chem. Lett. *20*, 3322–3325.
35. Gerke, V., and Moss, S.E. (2002). Annexins: from structure to function. Physiol. Rev. *82*, 331–371.
36. Sharma, M.C. (2019). Annexin A2 (ANX A2): an emerging biomarker and potential therapeutic target for aggressive cancers. Int. J. Cancer *144*, 2074–2081.
37. Feng, X., Liu, H., Zhang, Z., Gu, Y., Qiu, H., and He, Z. (2017). Annexin A2 contributes to cisplatin resistance by activation of JNK-p53 pathway in non-small cell lung cancer cells. J. Exp. Clin. Cancer Res. *36*, 123.
38. Takano, S., Togawa, A., Yoshitomi, H., Shida, T., Kimura, F., Shimizu, H., Yoshidome, H., Ohtsuka, M., Kato, A., Tomonaga, T., et al. (2008). Annexin II overexpression predicts rapid recurrence after surgery in pancreatic cancer patients undergoing gemcitabine-adjuvant chemotherapy. Ann. Surg. Oncol. *15*, 3157–3168.
39. Chu, Y.W., Yang, P.C., Yang, S.C., Shyu, Y.C., Hendrix, M.J., Wu, R., and Wu, C.W. (1997). Selection of invasive and metastatic subpopulations from a human lung adenocarcinoma cell line. Am. J. Respir. Cell Mol. Biol. *17*, 353–360.
40. Subramanian, A., Tamayo, P., Mootha, V.K., Mukherjee, S., Ebert, B.L., Gillette, M.A., Paulovich, A., Pomeroy, S.L., Golub, T.R., Lander, E.S., and Mesirov, J.P. (2005). Gene set enrichment analysis: a knowledge-based approach for interpreting genome-wide expression profiles. Proc. Natl. Acad. Sci. U S A *102*, 15545–15550.
41. Cline, M.S., Craft, B., Swatloski, T., Goldman, M., Ma, S., Haussler, D., and Zhu, J.C. (2013). Exploring TCGA pan-cancer data at the UCSC cancer genomics. Browser. Sci. Rep. *3*, 2652.
42. Camp, R.L., Dolled-Filhart, M., and Rimm, D.L. (2004). X-tile: a new bio-informatics tool for biomarker assessment and outcome-based cut-point optimization. Clin. Cancer Res. *10*, 7252–7259.
43. Gyorffy, B., Surowiak, P., Budczies, J., and Lanczky, A. (2013). Online survival analysis software to assess the prognostic value of biomarkers using transcriptomic data in non-small-cell lung cancer. PLoS One *8*, e82241.